Electronic Supplementary Material (ESI) for Physical Chemistry Chemical Physics.
This journal is © the Owner Societies 2020

Supplementary Information: Role of Image Charges in Ionic Liquid Confined between Metallic Interfaces

Samuel Ntim and Marialore Sulpizi*

Institut für Physik, Johannes Gutenberg Universität, Staudingerweg 7, 55128-Mainz, Germany

E-mail: sulpizi@uni-mainz.de

Contents

MD Simulation setup and details

Electrode systems

We built up a system of 1200 pairs of [BMIM][BF_4] confined in two slabs of either non-polarisable or polarisable gold. Unlike the non-polarisable gold which interact purely through Lennard-Jones potentials, a single polarisable gold "atom" consists of two masses of equal charge magnitudes but of opposing signs, so to give a zero total charge. The one mass of 195.96 u represents all of a gold atom (core) but its outermost deformable electron cloud, represented by the other mass of 1.00 u (shell). Each mass has a charge of magnitude 1.0 e, the core being positive while the shell negative. The two masses are bonded by a harmonic potential with a stiffness $k_r = 100.0\,\mathrm{kcal\,mol^{-1}\,Å^{-2}}$ and with no separation when no external forces exist, $r_0 = 0.0\,\mathrm{Å}$. The Lennard-Jones parameters are

$$\sigma_{ii} = 2.6246\,\mathrm{Å} \qquad \epsilon_{ii} = 3.5\,\mathrm{kcal\,mol^{-1}}$$

for the one mass representing the core and

$$\sigma_{ii} = 2.6246\,\mathrm{Å} \qquad \epsilon_{ii} = 0.2\,\mathrm{kcal\,mol^{-1}}$$

for the shell. We use the Lorentz-Berthelot combination rules for interactions between unidentical atoms

$$\epsilon_{ij} = \sqrt{\epsilon_{ii}\epsilon_{jj}} \qquad \sigma_{ij} = \frac{\sigma_{ii} + \sigma_{jj}}{2}.$$

The full interaction potential between the masses is

$$V = \frac{1}{2} \sum_{bonds} k_r \left(r - r_0\right)^2 + \sum_{i<j} 4\epsilon_{ij} \left(\frac{\sigma_{ij}^{12}}{r_{ij}^{12}} - \frac{\sigma_{ij}^{6}}{r_{ij}^{6}} \right) - \frac{q_i q_j}{r_{ij}} \tag{1}$$

Each slab was made of 9 layers of gold atoms in the (111) crystallographic plane. Five independent starting configurations of the ionic liquid confined in the slabs were sampled from an NPT run performed for 20 ns using a Nosé-Hoover thermostat at 298 K and semi-isotropic Berendsen barostat at 1 bar with compressibility only in the z-axis and with 3D periodic boundary conditions. Then NVT production runs were performed with each of the five starting configuration for 50 ns using a velocity rescale thermostat at 298 K. The systems were evolved at 0.5 fs timesteps and integrated with the leap-frog algorithm, saving information every 1000 molecular dynamics steps (0.5 ps). In such highly Coulombic systems, and for the purposes of this study, inclusion of long range Coulomb interactions was crucial. We employ the Particle Mesh Ewald (PME) with correction to slab geometries developed by Yeh and Berkowitz.[1] The slab geometry correction required vacuum of about three times (or more) of the system length, between the slabs, outside of the confining region. We used $4.054\,57 \times 4.054\,57 \times 250\,\mathrm{nm}^3$ as our simulation box dimensions in the production run, allowing for vacuum of 222 nm.

Work of adhesion

We calculated the work of adhesion using the dry surface approach by Leroy and Mulle-Plathe.[2] In this scheme the calculation required a slightly different setup, that is, a single [BMIM][BF_4]-Gold interface. In particular we calculated two values of the work of adhesion, namely one corresponding to the wall-liquid interface and the other corresponding to the wall-solid interfaces. In the case of the wall-liquid, we used a system of one gold slab in contact with the liquid of 400 pairs of [BMIM][BF_4] with box dimensions $4.054\,57 \times 4.054\,57 \times 50\,\mathrm{nm}^3$. 2 ns NVT runs were performed for 26 points along each cou-

pling parameter axis shown in Figure 3, using the last configuration at one point as the starting configuration at the next point along the coupling parameter axis. Points were chosen to be denser near $\sqrt{\epsilon_s} = 0.0\,\sqrt{\mathrm{kJ/mol}}$. For each run, the temperature was kept at 298 K using a velocity rescale thermostat and electrostatics were calculated using PME with correction to slab geometries.[1] Lennard-Jones interactions were calculated using a cut-off of 1.5 nm and a potential shift with Verlet cut-off scheme, and the dispersion correction to the energy and pressure[3] as implemented in GROMACS 5.1.4.

The systems were evolved at 0.5 fs timesteps and integrated with the leap-frog algorithm, saving information every 0.5 ps. Similar system with 3400 molecules of SPC/E water was used in calculating the reference work of adhesion (blue line in Figure 3 (A)).

In order to estimate the shift in temperature we calculated also the work of adhesion γ_{sw} for the solid-wall interaction. Using the setup from the previous calculation of work of adhesion, we randomise the molecules by raising the temperature from 298 K to 500 K over 1 ns and then anneal to 150 K over 2 ns, after which the temperature was maintained at 150 K for 2 ns. We used then the final configuration to perform the free energy calculations at 150 K, keeping all other parameters the same as for the calculations at 298 K.

Figure S1 shows the density of the system over the course of freezing, in the region shown in the inset.

Layering and local structure

Figure S2 shows the ion number densities and the total mass densities (inset) for systems with polarisable and non-polarisable gold. We observe that from the gold surfaces the liquid retains a strong interfacial structure only to be lost beyond 2 nm from surfaces. The lines for the non-polarisable (black) and polarisable (red) models are basically indistinguishable, even when comparing cation and anion density distributions separately.

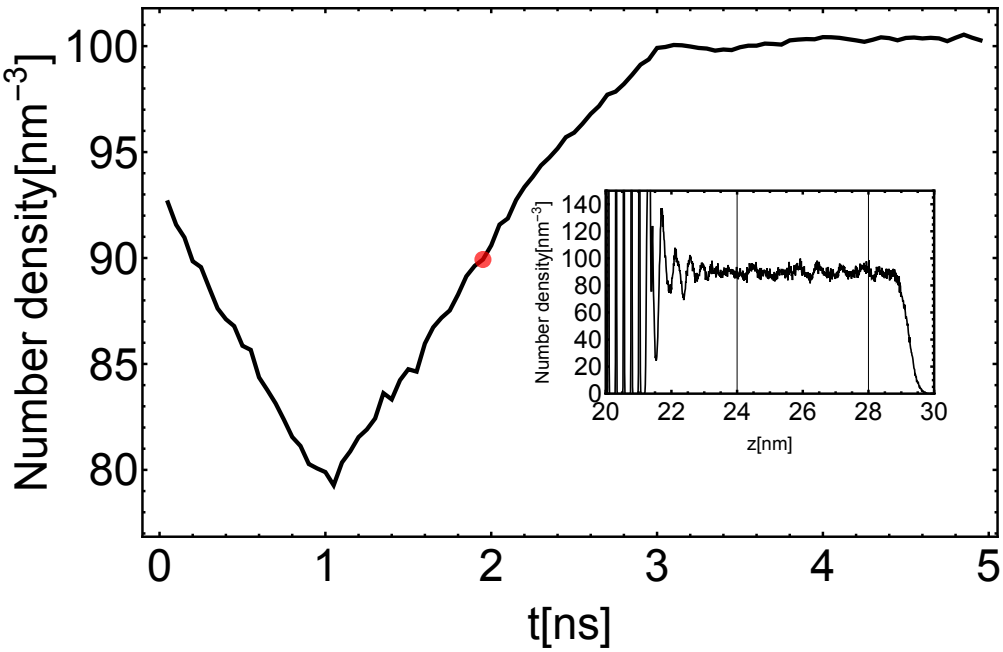

Figure S1: Density of ionic liquid during freezing. The inset shows an example density profile, corresponding to the red point, where the vertical lines show the region from which the number density is obtained.

It is also seen in Figure S3, which shows a close up of the ion densities at the interface in Figure S2, that cations, shown in solid lines, adsorb slightly closer (about 2.4 Å) to the gold than anions, shown in dashed lines, and is similar for both non-polarisable (in black lines) and polarisable (in red lines) gold systems. The more flat and elongated shape of the cations permits them to maximise the number of van der Waals contacts with the surface, thus adsorbing closer to the surface. Nonetheless, as a compensation and due to the relatively higher packing of the anions, there is an excess of anions peaking earlier at the interface (at 2.8 Å) than cations (at 2.95 Å).

We also examine the orientation of cations across the interface following the scheme presented by Ferreira et al.[4] Normalised distributions of orientation of cations in the first adsorption layer on non-polarisable and polarisable gold surfaces are shown in Figure S4. (A) shows the normalised distribution of angles formed by the axis across the imidazolium ring from the methyl carbon to the first butyl carbon (blue axis), and the normal to the gold surface (yellow axis). The preferred orientation is with the two axis almost perpendicular

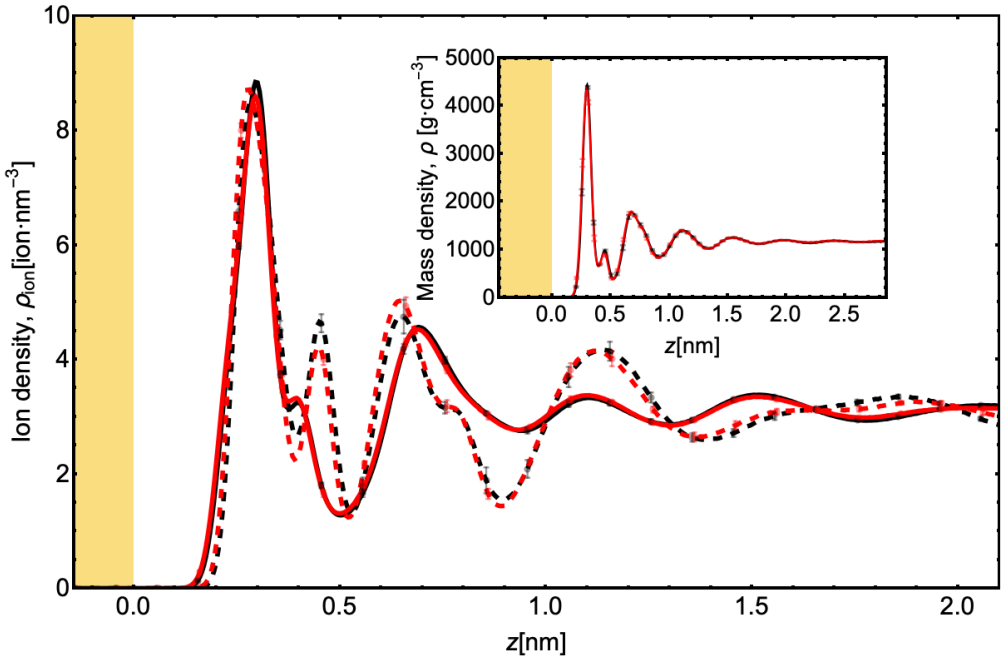

Figure S2: Liquid exhibits strong structure at the interface that extends to about 2 nm from the non-polarisable gold surface (black) and also from the polarisable gold surface (red). The inset shows the liquid mass densities where the extent of the liquid interfacial structure is shown much clearly.

to each other. (B) shows the normalised distribution of angles formed by the normal to the gold surface (yellow axis) and the vector from the first butyl carbon to the last butyl carbon (blue axis). (C) shows the orientation of the plane of the imidazolium ring (major blue axis, which is a cross product of the two minor blue axes) with respect to the normal to the surface (yellow axis). Thus, the cations in the first adsorbed layer mainly bind to the surface maintaining their imidazole ring parallel to the Au(111) surface (Figure S4). A similar result was also found in SFB experiments (Perkin et al.[5]) for [EMIM][$EtSO_4$] confined between mica sheets, where the aromatic rings of [EMIM] were also shown to align parallel to the mica surface. Indeed, such preferred alignment is expected even for rather simplified ionic liquid models at neutrally charged electrodes as demostrated by Breitsprecher et al.,[6,7] with the probability of having such orientation increasing with the surface charge on the electrodes. In contrast to this well-defined orientation in the first adsorption layer, Figure S5 also shows that there is no preferred orientation of the cation

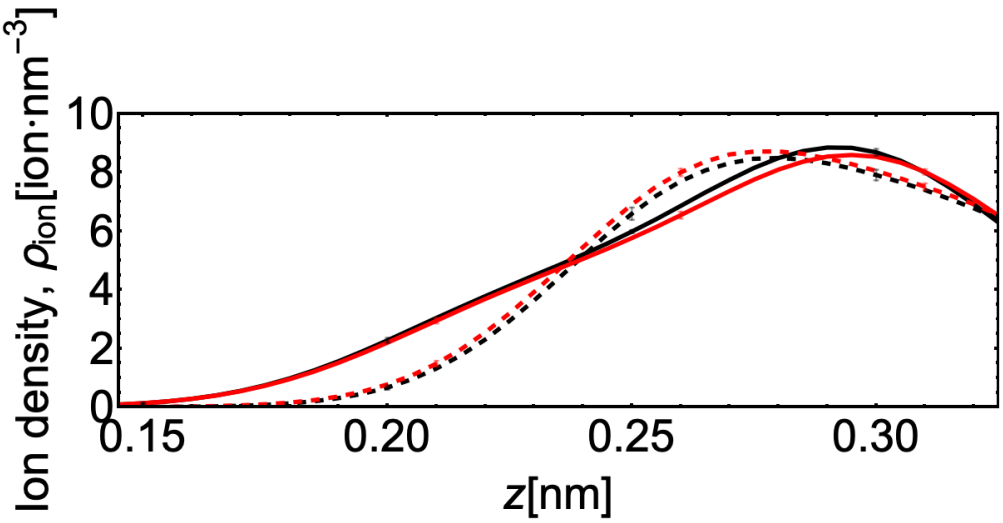

Figure S3: Cations (solid lines) adsorb closer to the gold than anions (dashed lines). The results for the non-polarisable model are reported in black, while those for the polarizable model are reported in red.

beyond the first layer and that the orientation becomes completely random already at about 10 Å from the gold surface.

Using the x- and y-coordinates of their centres of mass, the pair correlation functions (shown in Figure S6) calculated between imidazolium of cations, and anions show strong counterion peaks at about 0.502 nm radius. This feature weakens going into the bulk. Bulk structures are recovered after about 1.9 nm (yellowest lines), confirming the recovery of bulk shown by density profiles in Figure S2.

To further demonstrate that the metal polarisation induces only a subtle difference in the layering of the liquid, we analyse the variation in the charge densities in the liquid across the interface.

$$\rho_{q,j}(n\Delta z) = \sum_{i \in j} q_i \rho_{N,i}(n\Delta z) \tag{2}$$

where q_i is the charge of atoms of type i in a molecule of type j. The adsorption of the cation at the surface builds up an excess of positive charge also shown by the first peak in the cation charge distribution (Figure S7). In response, the smaller anions, having a

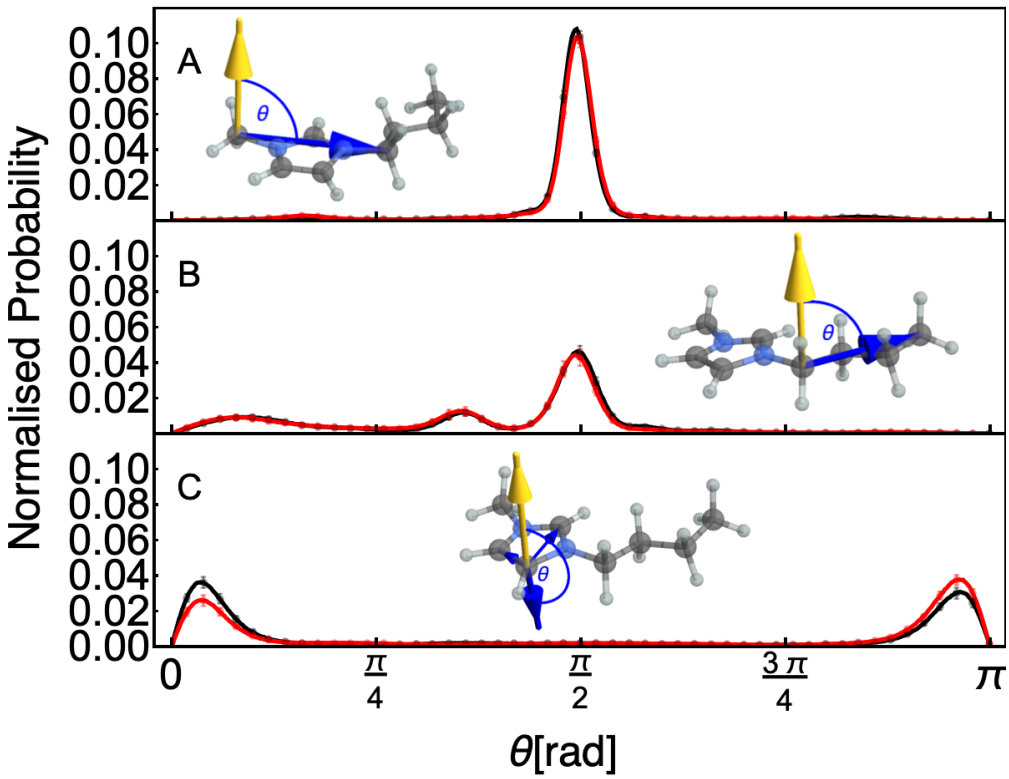

Figure S4: Normalised distribution of orientation of cations in the first adsorption layer. (A) Tilt of the ring head (B) Tilt of the butyl tail (C) Tilt of the plane in which lies the ring.

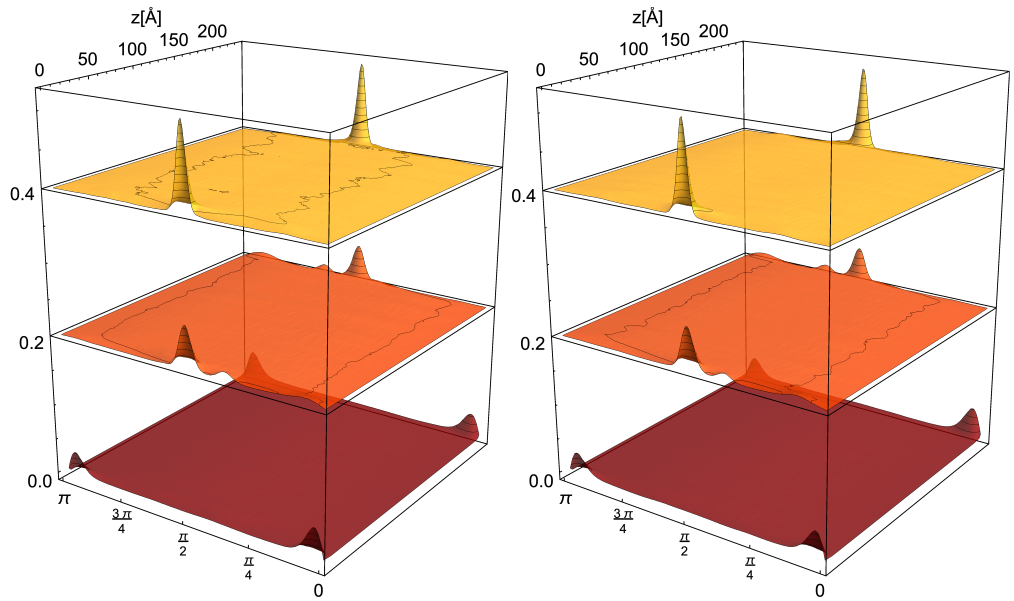

Figure S5: Evolution of cation orientation along the z-axis for non-polarisable (left) and polarisable (right) gold. The distributions have been shifted for clarity. Features of the distribution of angles in Figure S4 only persist within the first 10 Å from the surface.

higher packing density at the interface, accumulate in the next layer and overcompensate the excess charge from the cations. A slightly positively charged layer follows as next, after which charge fluctuations extend up to 2 nanometers from the Au(111) surface (Figure S7). A similar charge density distribution was found in the case of [BMIM][PF_6] and [BMIM][TNf_2] by Ferreira et al.[4]

Figure S7 shows the charge densities of the ions and their sums. In the inset is the electric field, showing clearly the extent of the influence of the interface. It can also be seen that the fluctuations in the charge density, and hence the electric field, are strongly influenced by the anions. Note that the positive peak (around 3.5 Å) for the anions, surrounded by negative peaks, is from the positively charged boron ion of the anion. The two negative peaks that surround this positive peak are from the tetrahedral arrangement of fluoride ions around the boron ion.

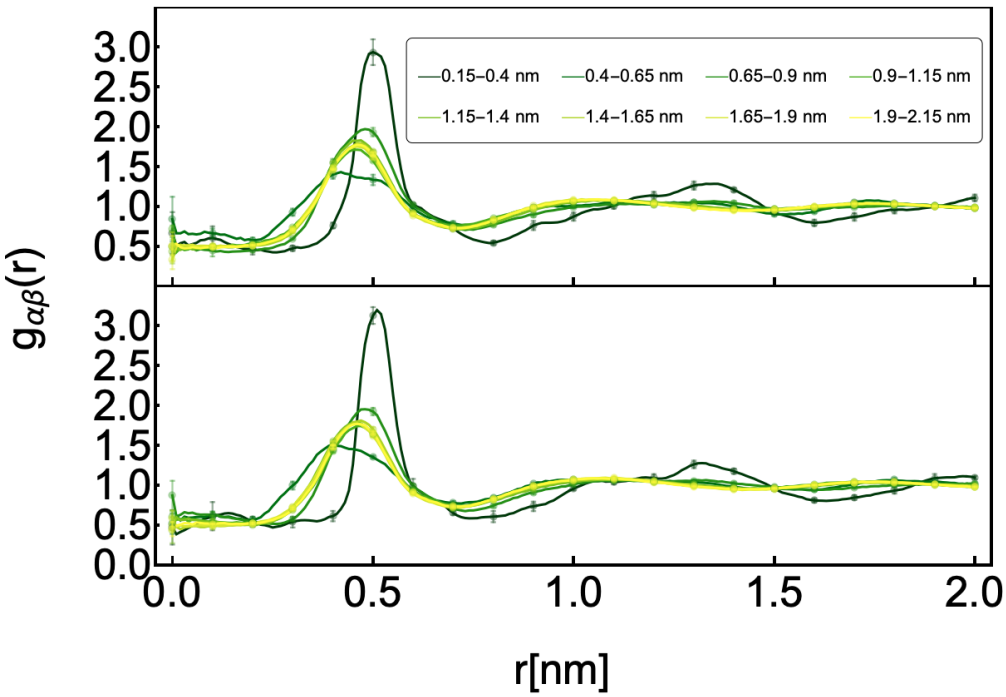

Figure S6: Pair correlation functions of centre of mass of imidazolium of cation and centre of mass of anion, calculated within regions of 0.25 nm width across the interface with non-polarisable (top) and polarisable (bottom) gold. Dark green and yellow correspond to regions at the interface and in bulk, respectively.

Diffusion coefficient

Dividing the interface into symmetrised regions, the 2-dimensional diffusion coefficient D_α in a region α over a duration τ is calculated with the Einstein

$$D_\alpha = \frac{1}{4} \lim_{\tau \to \infty} \frac{\mathrm{d}}{\mathrm{d}\tau} \mathrm{MSD}_\alpha(\tau) \tag{3}$$

where MSD_α is the mean squared displacement in the region α, defined, for example along the x-axis and with a reference time t, as

$$\mathrm{MSD}_{x,\alpha}(t,\tau) = \frac{\sum_i \sigma_{i,\alpha}(t)\sigma_{i,\alpha}(t+\tau)(x_i(t+\tau) - x_i(t))^2}{\sum_i \sigma_{i,\alpha}(t)\sigma_{i,\alpha}(t+\tau)} \tag{4}$$

where $\sigma_{i,\alpha}(t)$ is a switching function for the ith particle in the region α at time t, and $x_i(t)$ is the coordinate of the ith particle at time t. Then by restarting the calculation of $\mathrm{MSD}_{x,\alpha}(t,\tau)$

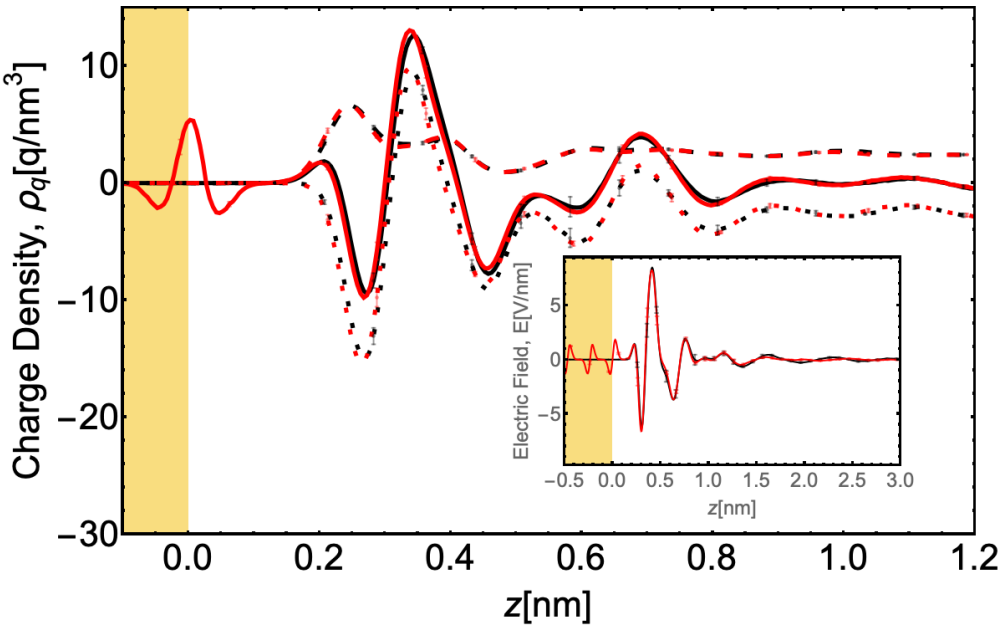

Figure S7: Distribution of charge on non-polarisable gold (black) and polarisable gold (red) surfaces across the interface. Dotted lines are densities for anions, dashed lines, those of cations and continous lines, their sums. The inset shows the integral of charge distribution, the electric field.

at different reference times,

$$\mathrm{MSD}_\alpha(\tau) = \frac{1}{N}\sum_{n=1}^{N}\sum_{j\in\{x,y\}} \mathrm{MSD}_{j,\alpha}(n\Delta t, \tau) \tag{5}$$

where Δt is a restart time (the time between two successive reference times) and N, the number of restarts. For each of the five independent trajectories, skipping the first 10 ns, the subsequent 40 ns were divided into 16 consecutive parts. MSD with $\tau = 2.5$ ns was calculated with a 10 ps restart time for each part and then averaged over all 16. The diffusion coefficients for each region were then calculated according to Equation 3, taking slopes of the MSDs between $\tau = 0.25$ ns and $\tau = 1$ ns, and then averaged over all five trajectories. Figure

In the calculation of the D_α the size correction[8] was ignored. Using the dimensions of our system, $L_\perp = 23.7$ nm and $L_\parallel = 4.054\,57$ nm we find that $h_\parallel \approx 5.046$, and with bulk viscosity $\eta \approx 150$ mPa s at temperature of $T = 298$ K, we find that the correction to the

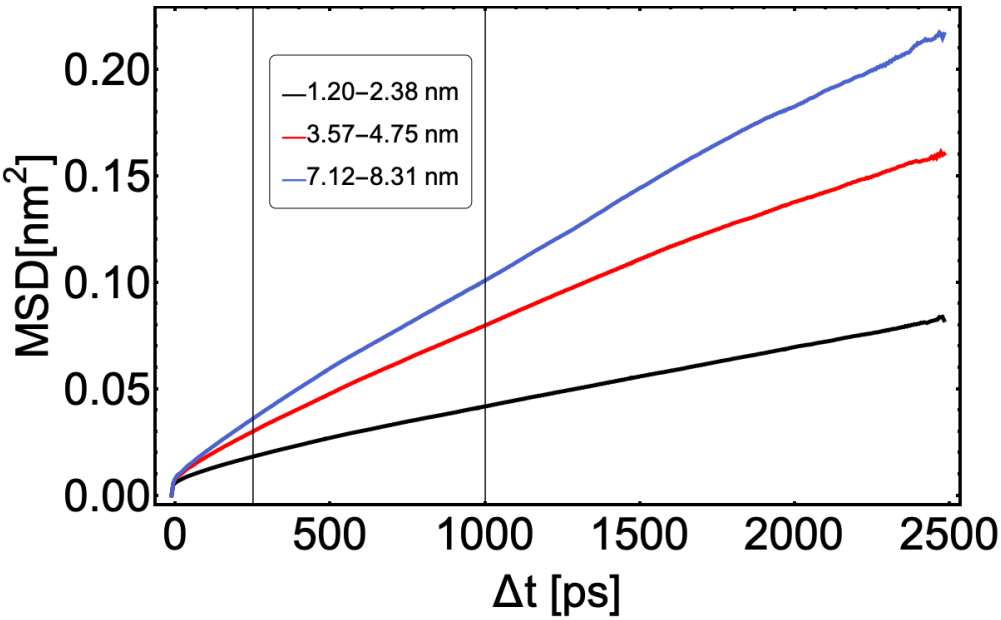

Figure S8: MSD for cations found in three regions. Vertical lines show portions of MSD used in calculation of corresponding D_α.

diffusion coefficient

$$\Delta D_{\parallel} = -\frac{k_B T}{6\pi\eta L_{\parallel}} h_{\parallel} \tag{6}$$

$$= -1.811 \times 10^{-12}\,\mathrm{m^2\,s^{-1}} \tag{7}$$

is insignificant with respect to calculated D_α's. Similarly, for the bulk ionic liquid with isotropic box size $L = 6.355\,\mathrm{nm}$, we find that the correction to the diffusion coefficient[9] is

$$\Delta D_{bulk} = \frac{k_B T}{6\pi\eta L}\xi \tag{8}$$

$$= 6.5 \times 10^{-13}\,\mathrm{m^2\,s^{-1}} \tag{9}$$

where $\xi = 2.837297$.

Unlike what is found from the structural properties, the effect of the interface is much more extended on the dynamics. The diffusion coefficients of both species of ions gradually evolves to bulk value. For that reason, the choice of the system size is crucial, in order to

correctly calculate the diffusion coefficients. For example, Figure S9 shows the diffusion coefficients of the cations for systems of 400, 800 and 1200 pairs. In each of these three systems the lateral (x, y) dimensions are kept constant to $4.054\,57 \times 4.054\,57\,\mathrm{nm}^2$ while the distance between the two gold surfaces along the z is increased. Comparing the smaller system of 400 pairs to the larger systems, it is interesting to notice that the slope of the curves near the interface shows that diffusion near the interface is also affected by the size.

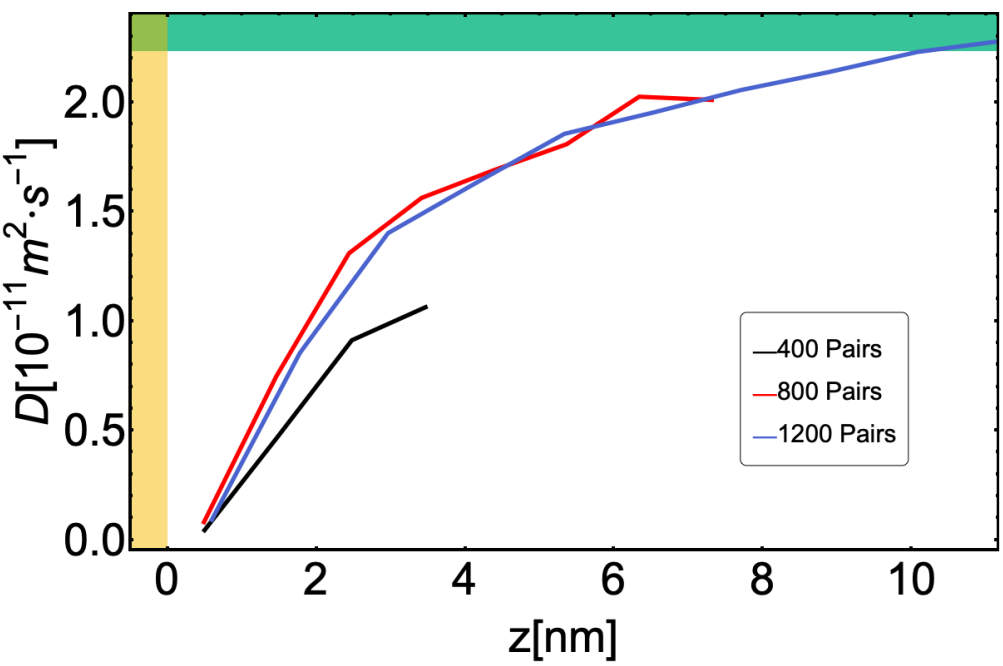

Figure S9: Effect of system size on the self-diffusion of cations. One recovers the bulk value for the largest system (1200 pairs. The bulk value for the diffusion coefficient, calculated from the simulations, is reported as green strip, along with the error bar.

The diffusion coefficients of the ions in Figure 4, fitted to the exponential function

$$f(z) = k\left(1 - e^{-(z-\zeta)/\lambda}\right) \tag{10}$$

give the characteristic lengths λ shown in TABLE SI. Figure S10 shows the exponential fit curves (shown in thin lines) to the self-diffusion of ions across the interface in the system with non-polarisable gold (shown in black lines) and polarisable gold (shown in red lines)

Table SI: Table of exponential fit parameters.

	ζ/nm	$k/10^{-11}\,\mathrm{m^2\,s^{-1}}$	λ/nm
		BMIM	
Non-polarisable gold	0.45	2.28	2.9
Polarisable gold	0.45	2.56	3.6
		BF_4	
Non-polarisable gold	0.52	1.68	3.5
Polarisable gold	0.51	1.90	4.5

surfaces.

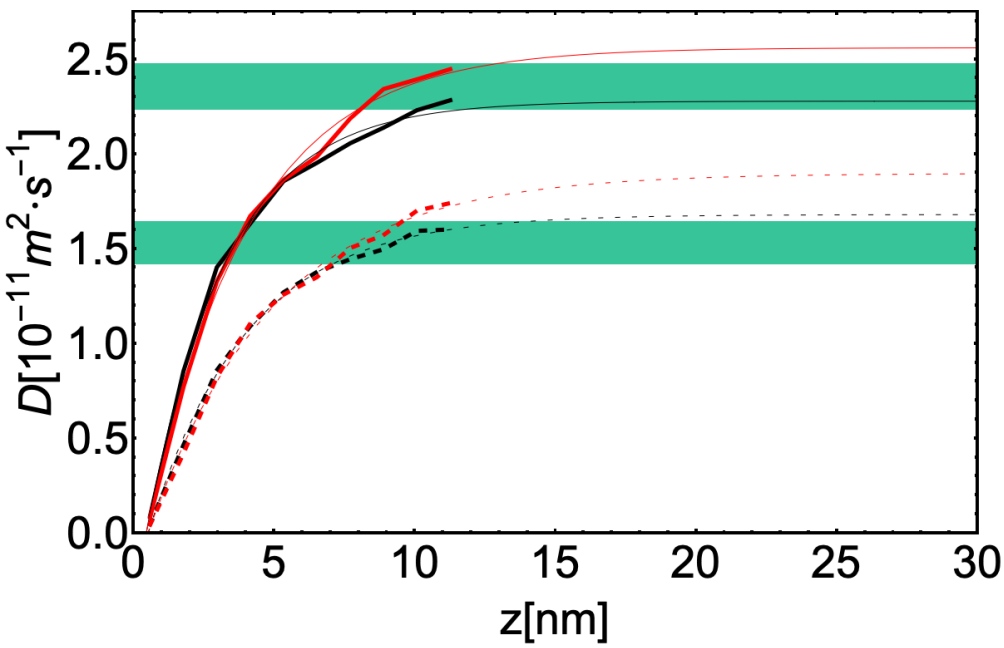

Figure S10: Exponential fit to the self-diffusion of ions in systems with non-polarisable gold (black) and polarisable gold (red) surfaces. Thin lines correspond to the fitted curves while thick lines correspond to the data. Dashed lines correspond to anions while those of cations are continous lines.

References

(1) Yeh, I.-C.; Berkowitz, M. L. Ewald summation for systems with slab geometry. *J. Chem. Phys.* **1999**, *111*, 3155–3162.

(2) Leroy, F.; Muller-Plathe, F. Dry-surface simulation method for the determination of the work of adhesion of solid–liquid interfaces. *Langmuir* **2015**, *31*, 8335–8345.

(3) Allen, M. P.; Tildesley, D. J. *Computer Simulation of Liquids*, 2nd ed.; Oxford University Press, Inc.: USA, 2017.

(4) Ferreira, E. S. C.; Pereira, C. M.; Cordeiro, M. N. D. S.; dos Santos, D. J. V. A. Molecular Dynamics Study of the Gold/Ionic Liquids Interface. *J. Phys. Chem. B* **2015**, *119*, 9883–9892.

(5) Perkin, S.; Albrecht, T.; Klein, J. Layering and shear properties of an ionic liquid, 1-ethyl-3-methylimidazolium ethylsulfate , confined to nano-films between mica surfaces. *Phys. Chem. Chem. Phys.* **2010**, *12*, 1243–1247.

(6) Breitsprecher, K.; Košovan, P.; Holm, C. Coarse-grained simulations of an ionic liquid-based capacitor: I. Density, ion size, and valency effects. *J. Phys.: Condens. Matter* **2014**, *26*, 284108.

(7) Breitsprecher, K.; Košovan, P.; Holm, C. Coarse-grained simulations of an ionic liquid-based capacitor: II. Asymmetry in ion shape and charge localization. *J. Phys.: Condens. Matter* **2014**, *26*, 284114.

(8) Botan, A.; Marry, V.; Rotenberg, B. Diffusion in bulk liquids: finite-size effects in anisotropic systems. *Molecular Physics* **2015**, *113*, 2674–2679.

(9) Yeh, I.-C.; Hummer, G. System-size dependence of diffusion coefficients and viscosities from molecular dynamics simulations with periodic boundary conditions. *J. Phys. Chem. B* **2004**, *108*, 15873–15879.